Eidgenössische Technische Hochschule Zürich

Ecole polytechnique fédérale de Zurich
Politecnico federale di Zurigo
Swiss Federal Institute of Technology Zurich

An adaptive finite element method for distributed heat flux reconstruction

J. Li, J. Xie* and J. Zou†

Research Report No. 2010-23
August 2010

Seminar für Angewandte Mathematik
Eidgenössische Technische Hochschule
CH-8092 Zürich
Switzerland

*Department of Mathematics, Shanghai Jiao Tong University, Shanghai 200240, China. The work of this author was partly supported by the NSF of China (No.10801098) and the E-institute of Shanghai Municipal Education Commission (N.E03004).

†Department of Mathematics, The Chinese University of Hong Kong, Shatin, N.T., Hong Kong. The work of this author was substantially supported by Hong Kong RGC grants (Projects 404407).

An Adaptive Finite Element Method for Distributed Heat Flux Reconstruction

Jingzhi Li * Jianli Xie † Jun Zou ‡

August 17, 2010

Abstract

Based on a posteriori error estimates, we propose an adaptive finite element method for a distributed heat flux reconstruction in a stationary heat conductive system, namely recovering the unknown distributed flux on some inaccessible boundary using partial measurement data on other accessible boundaries. A posteriori error estimates are first derived. Efficiency of the derived error estimator is addressed by showing that the error estimator provides upper and lower bounds on the discretization errors of quantities of interest, up to some constants. It is revealed for the first time that the constant of the upper bound depends explicitly on the regularization parameter, which could be essential for employing adaptive techniques to inverse problems. Numerical experiments are presented to show the applicability and efficiency of the proposed adaptive method based on the derived error estimator.

Key Words: Inverse problems, regularization, adaptive finite element method, a posteriori error estimates, distributed heat flux reconstruction

AMS subject classification 2000: Primary 65M30; Secondary 35R30, 65M60

1 Introduction

In assorted engineering disciplines, inverse problems arise naturally from optimal design, control, identification and reconstruction processes. Inverse theory has witnessed great success during the past few decades. In this paper, we are interested in the adaptive reconstruction of the distribution of the unknown heat flux on some inaccessible part of the boundary in a stationary heat conductive system, from the partial measurements on other accessible part of the boundary.

The heat flux distribution are of immense practical interest in thermal and heat transfer problems, e.g., the real-time monitoring in metallurgical industry [2] and the visualization by liquid crystal thermography [9]. But its accurate distribution is rather difficult to obtain on some inaccessible boundary, such as the interior boundary of nuclear reactors and steel furnaces. Instead engineers attempt to recover the heat flux from some measured data, which leads naturally to the inverse problem of reconstructing the distributed heat flux from the measurements on the accessible part of the boundary. This inverse problem is essentially ill-posed in Hardamard's sense [11] that at least one of three conditions, namely existence, uniqueness and continuous dependence on the given data, does

*SAM, Department of Mathematics, ETH Zürich, CH-8092 Zürich, Switzerland (jingzhi.li@sam.math.ethz.ch).

†Department of Mathematics, Shanghai Jiao Tong University, Shanghai 200240, People's Republic of China (xjl@sjtu.edu.cn). The work of this author was partly supported by the NSF of China (No.10801098) and the E-institute of Shanghai Municipal Education Commission (N.E03004).

‡Department of Mathematics, The Chinese University of Hong Kong, Shatin, N.T., Hong Kong (zou@math.cuhk.edu.hk). The work of this author was substantially supported by Hong Kong RGC Grant (Project 404407).

not hold. Some other optimal design problems may give rise to similar inverse problems too, e.g., the freezing front velocity (represented by the Neumann boundary flux) needs to be determined in the solidification process [22].

Several numerical methods have been proposed for the distributed heat flux reconstruction problem, among which the least-squares formulation [21, 22, 23] has received intensive investigations and it has been implemented by means of the boundary integral method [23] and finite element method [21]. Nonetheless, the numerical reconstruction of the distributed heat flux studied in the literature so far is done using globally quasi-uniform meshes (see, e.g., [21]), that either smears out the local but potentially very important feature of the distributed heat flux on a coarse mesh or demands formidable computational cost for high resolution of such local feature on a very fine regular mesh.

Local characteristics appear frequently and naturally in practical applications, e.g., non-smooth boundaries, discontinuous heat fluxes, or singular heat fluxes with spikes or abrupt sign changes. These unpredictable local features of the unknown heat flux poise demanding challenges for any effective numerical reconstruction. In this paper, we focus on the adaptive retrieval of local characteristics in the way that local features are automatically captured using adaptive finite element methods (AFEMs) based on the a posteriori error estimation.

AFEMs based on a posteriori error estimates have been extensively investigated after the seminal paper by Babuška and Rheinboldt [3] in the late 1970s. The pivotal question in AFEM is how to measure, control and effectively minimize the discretization error of quantities of interest based on the computed solution and given data. The AFEM automatically enhances the resolution of the numerical solution by increasing the number of degrees of freedom in certain regions of the computational domain, where the true solution is hard to be approximated, e.g., around the reentrant corner or places with singularity. Remarkable success of theories and methods of a posteriori error estimation has opened a new era in scientific computation and numerical analysis. Global and local information to assess the accuracy of the discretization error of the numerical solution can be obtained to guide local adaptive mesh refinement by using the computational quantities in terms of the numerical solution itself and the specified data of the problem under concerns. Readers may refer to two monographs for some typical direct problems by Ainsworth-Oden [1] and Verfürth [20] and references therein.

AFEMs have witnessed significant advances in reducing the computational complexity and improving efficiency of problems in the solution of a variety of direct partial differential equations. On the contrary, adaptive theory and methods for inverse problems are still in its infancy. Some recent efforts on adaptive methods for inverse or PDE-constrained optimization problems include 1) the dual weighted residual framework in terms of some quantity of interest [4, 5, 6], which provides a general recipe to solve inverse problems; 2) adaptive parameter identification in elliptic system [10]; and 3) adaptive methods for PDE-constrained optimal control problems [14, 16, 17], to mention a few.

Nevertheless, there are some potential limitations on the adaptive inverse techniques mentioned above. In [4, 5, 6], the adaptive strategy is guided by a so-called quantity of interest with error estimation derived from the dual weighted residual framework. The a posteriori error estimators are based solely on the computed quantity of the control variable and given data, which evidently neglects all discretization errors from the state and adjoint variables and could be thus biased and insufficient. Moreover, their error estimators are derived by ignoring the higher order terms in the truncation of the Lagrangian functional. These higher order terms should be incorporated in the a posteriori error estimator for saturated estimation. In particular in the initial stages of an adaptive algorithm, the mesh sizes are often not really small and hence these terms are not negligible at all. In [10], the a posteriori error estimators are derived using a traditional residual based error estimates. The error estimates for all control, state and costate variables are obtained. However, to derive the a posteriori error estimates, the convexity of the least-squares cost functional is assumed and hence the regularization parameter is expressed in the upper bound constant in an implicit way, which hinders further insight into possible relative relation between the discretization error and the a posteriori error estimator. Moveover, the requirement of regularity for the control variable is high, which rules out

some physically interesting cases. In addition, the global $W^{1,\infty}$-norm of the computed solution is implicitly absorbed in the generic constant in the estimates.

Our aim in this paper is to propose an adaptive finite element method for the inverse problem of reconstructing the distributed heat flux on the inaccessible part of the boundary from partial measurements on the accessible part of the boundary. Keeping the regularity assumption reasonably low, we shall derive rigorously the a posteriori error estimates for control, state and costate variables. The estimators are shown to be optimal in the sense that they provide both upper and lower bounds of the discretization error, up to some constants. It is revealed for the first time that the constant in the upper bound depends explicitly on the regularization parameter, which could be essential for employing adaptive techniques to inverse problems formulated by the least-squares formulation with Tikhonov regularization.

The paper is organized as follows. In section 2, we describe our heat flux reconstruction problem and formulate it as a stabilized nonlinear optimization problem by defining a least-squares cost functional with Tikhonov regularization. We propose the finite element discretization and analyze some important properties of the mathematical formulation. In section 3, a posteriori error estimates for the finite element approximation of the heat flux reconstruction problem are derived, which are further proved to be able to serve as upper and lower bounds of the discretization error up to some constants. In section 4, numerical experiments are presented to show the applicability and efficiency of the proposed adaptive method for the distributed heat flux reconstruction based on the derived error estimator. A key observation is that although the regularization parameter seems playing an adverse amplification role in characterizing the upper bound of the discretization errors, the error estimator always provides accurate locations of elements for the next refinement, which captures the singularity of the parameters very effectively. We conclude the work and point out some future directions in Section 5.

We end this section with some notations and conventions. Throughout the paper we adopt the standard notation $W^{m,p}(D)$ for Sobolev spaces on D, and $H^m(D) = W^{m,2}(D)$. Here D can be a subset of some bounded polygonal or polyhedral domain $\Omega \subset \mathbb{R}^d$ $(d = 2, 3)$, or a subset of the boundary $\Gamma = \partial\Omega$. The norm and semi-norm in $H^m(D)$ are denoted respectively by $\|\cdot\|_{m,D}$ and $|\cdot|_{m,D}$. We use $(\cdot,\cdot)_D$ to denote the inner product in $L^2(D)$. If $D = \Omega$, we may simply drop D in the notation $\|\cdot\|_{m,D}$ and $(\cdot,\cdot)_D$. In addition, we will often use c or C to denote generic positive constants which are independent of mesh size h and functions involved.

2 Mathematical formulation of the inverse problem

We shall consider the stationary heat conductive equation

$$\begin{cases} -\nabla\cdot(\alpha\nabla u) = f(x), \ x \in \Omega, \\ -\alpha\dfrac{\partial u}{\partial n} = k(u - u_a(x)), \ x \in \Gamma_a, \\ -\alpha\dfrac{\partial u}{\partial n} = q(x), \ x \in \Gamma_i, \end{cases} \tag{2.1}$$

where the given data include the heat source f, the ambient temperature u_a, the heat transfer coefficient k and the diffusivity coefficient α. The boundary Γ of domain Ω is assumed to be formed by two sections, the accessible part Γ_a and the inaccessible part Γ_i, namely $\Gamma = \Gamma_a \cup \Gamma_i$.

Now we can formulate the inverse problem to be considered as follows:

(IP) Given the partial measurement data $z(x)$ of $u(x)$ on the accessible part Γ_a, recover the distributed heat flux $q(x)$ on the inaccessible part Γ_i.

The heat flux reconstruction problem is severely ill-posed, one may refer to [21, Theorem 2.2] for a proof in the time dependent case which could be easily adapted in our current stationary setting.

To tackle with the ill-posedness of the reconstruction process and to numerically reconstruct the distributed heat flux in a stable way, we employ the output least-squares formulation combined with the Tikhonov regularization to determine $q(x)$ by minimizing the cost functional

$$J(q) = \frac{1}{2}\|u(q) - z\|^2_{0,\Gamma_a} + \frac{\beta}{2}\|q\|^2_{0,\Gamma_i} \tag{2.2}$$

over $q \in L^2(\Gamma_i)$. Here $u(q) : L^2(\Gamma_i) \to H^1(\Omega)$ represent the solution operator of the direct problem (2.1), which maps parameter q to solution u. Following [21, Theorem 2.2], one can see that the reconstruction process of parameter q is stabilized in the sense that the solution to (2.2) is stable with respect to the perturbation of noisy data. For the later analysis, we first discuss the following optimality conditions of the minimization problem (2.2).

2.1 Optimality conditions of the minimization problem

The regularized formulation (2.1)–(2.2) of our inverse problem is a nonlinear optimization problem whose necessary and sufficient optimality conditions can be stated in the following lemma.

Lemma 2.1. *The optimization problem* (2.1)–(2.2) *admits a unique solution* q. *And* q *is the minimizer if and only if there is a costate* $p \in H^1(\Omega)$ *such that the triplet* (u, p, q) *satisfies the following optimality conditions:*

$$\begin{cases} (\alpha\nabla u, \nabla\phi) + (ku, \phi)_{\Gamma_a} = (f, \phi) + (ku_a, \phi)_{\Gamma_a} - (q, \phi)_{\Gamma_i}, \quad \forall \phi \in H^1(\Omega), \\ (\alpha\nabla p, \nabla\phi) + (kp, \phi)_{\Gamma_a} = (u - z, \phi)_{\Gamma_a}, \quad \forall \phi \in H^1(\Omega), \\ (J'(q), w) = (\beta q - p, w)_{\Gamma_i} = 0, \ \forall w \in L^2(\Gamma_i). \end{cases} \tag{2.3}$$

Proof. The existence and uniqueness of minimizers can be proved by following the same line in [21, Theorem 2.2] with slight modifications.

It remains to prove (2.3). It is easy to see that the first equation in (2.3) is the variational form for the state variable $u(q)$, the second equation is for the costate $p(q)$, which is the adjoint equation for $u(q)$ with respect to the defect $u - z$, and the third equation is the necessary condition for the minimizer q. From the calculus of variation, the Gâteaux derivative $u'(q)(w)$ of u in the direction of $w \in L^2(\Gamma_i)$ solves

$$(\alpha\nabla u'(q)(w), \nabla\phi) + (ku'(q)(w), \phi)_{\Gamma_a} = -(w, \phi)_{\Gamma_i}, \quad \forall \phi \in H^1(\Omega)\,.$$

Combining this with the adjoint equation for $p(q)$, the Gâteaux derivative of functional J with respect to w can be computed as

$$\begin{aligned} J'(q)w &= (u - z, u'(q)(w))_{\Gamma_a} + \beta(q, w)_{\Gamma_i} \\ &= (\alpha\nabla p, \nabla u'(q)(w)) + (kp, u'(q)(w))_{\Gamma_a} + \beta(q, w)_{\Gamma_i} \\ &= (\beta q - p, w)_{\Gamma_i}. \end{aligned}$$

This completes the proof of Lemma 2.1. □

2.2 Finite element discretization of the inverse problem

We are now going to propose a fully discrete finite element scheme to approximate the continuous nonlinear optimization (2.1)–(2.2). Let T^h be a partition of Ω into disjoint open regular d-simplices τ so that $\bar{\Omega} = \cup_{\tau\in T^h}\bar{\tau}$ [8]. The natural restriction of T^h on the boundary of Ω forms the triangulations of Γ_i and Γ_a, denoted by Γ_i^h and Γ_a^h, respectively. Let F^h be the set of all faces of the triangulation T^h which are not on the boundary of Ω, namely, $F^h = \partial T^h \setminus (\Gamma_i^h \cup \Gamma_a^h)$. Let h_τ denote the diameter of the element τ in T^h, and h_l the diameter of the face l in ∂T^h. Associated with T^h is the piecewise linear

finite element subspace V^h of $C(\bar{\Omega})$. And we take the feasible approximation space for parameters q to be the natural restriction of V^h on the boundary Γ_i, denoted by $V^h_{\Gamma_i}$.

Then the continuous problem (2.2) can be discretized by the finite element approximation

$$\min_{q_h \in V^h_{\Gamma_i}} J_h(q_h) = \frac{1}{2}\|u_h(q_h) - z\|^2_{0,\Gamma_a} + \frac{\beta}{2}\|q_h\|^2_{0,\Gamma_i}, \tag{2.4}$$

where $u_h(q_h) \in V^h$ is the finite element discretization of (2.1), namely

$$(\alpha\nabla u_h, \nabla\phi_h) + (ku_h, \phi_h)_{\Gamma_a} = (f, \phi_h) + (ku_a, \phi_h)_{\Gamma_a} - (q_h, \phi_h)_{\Gamma_i}, \quad \forall \phi_h \in V^h. \tag{2.5}$$

As in Lemma 2.1, we can prove that there is a unique minimizer of (2.4)–(2.5) and that q_h is the minimizer of (2.4)–(2.5) if and only if there is a triplet $(u_h, p_h, q_h) \in V^h \times V^h \times V^h_{\Gamma_i}$ satisfying the optimality conditions:

$$\begin{cases} (\alpha\nabla u_h, \nabla\phi_h) + (ku_h, \phi_h)_{\Gamma_a} = (f, \phi_h) + (ku_a, \phi_h)_{\Gamma_a} - (q_h, \phi_h)_{\Gamma_i}, \quad \forall \phi_h \in V^h, \\ (\alpha\nabla p_h, \nabla\phi_h) + (kp_h, \phi_h)_{\Gamma_a} = (u_h - z, \phi_h)_{\Gamma_a}, \quad \forall \phi_h \in V^h, \\ (J_h'(q_h), w_h) = (\beta q_h - p_h, w_h) = 0, \ \forall w_h \in V^h_{\Gamma_i}. \end{cases} \tag{2.6}$$

3 A posteriori error estimates for the inverse problem

In this section we derive a posteriori error estimates for the finite element approximation (2.4)–(2.5) for our inverse problem. Before we proceed, some important technical lemmas are first introduced for the later derivation of the desired a posteriori error estimates.

Lemma 3.1. *Let I_h be the Scott-Zhang quasi-interpolation operator defined in [18]. For $s = 0, 1$ and $v \in H^1(\Omega)$, it holds that*

$$\|v - I_h v\|_{s,\tau} \le C \sum_{\bar{\tau}\cap\bar{\tau}'\neq\emptyset} h_\tau^{1-s}|v|_{1,\tau'}. \tag{3.1}$$

Lemma 3.2. (see [8]) *Let π_h be the standard Lagrange interpolation operator associated with V^h. For $m = 0, 1$ and $\forall v \in H^2(\Omega)$, we have*

$$\|v - \pi_h v\|_{m,\tau} \le C h_\tau^{2-m}|v|_{2,\tau}. \tag{3.2}$$

Lemma 3.3. (see [12]) *For all $v \in H^1(\Omega)$, it holds that*

$$\|v\|_{0,\partial\tau} \le C\big(h_\tau^{-1/2}|v|_{0,\tau} + h_\tau^{1/2}|v|_{1,\tau}\big). \tag{3.3}$$

3.1 A posteriori estimates: $L^2 - H^1$ norms

In this subsection, we establish the upper error bound for the error $q - q_h$ in L^2-norm and for the errors $u - u_h$ and $p - p_h$ in H^1-norm. We first introduce the following a posteriori errors:

$$\begin{aligned} \eta_1^2 &= \sum_{\tau\in T^h} h_\tau^2 \int_\tau |\nabla\cdot(\alpha\nabla p_h)|^2 dx, \quad \eta_2^2 = \sum_{l\in\Gamma_a^h} h_l \int_l \Big|\alpha\frac{\partial p_h}{\partial n} + kp_h - u_h + z\Big|^2 ds, \\ \eta_3^2 &= \sum_{l\in\Gamma_i^h} h_l \int_l \Big|\alpha\frac{\partial p_h}{\partial n}\Big|^2 ds, \quad \eta_4^2 = \sum_{l\in F^h} h_l \int_l [(\alpha\nabla p_h)\cdot n]^2 ds, \\ \zeta_1^2 &= \sum_{\tau\in T^h} h_\tau^2 \int_\tau |\nabla\cdot(\alpha\nabla u_h) + f|^2 dx, \quad \zeta_2^2 = \sum_{l\in\Gamma_a^h} h_l \int_l \Big|\alpha\frac{\partial u_h}{\partial n} + ku_h - ku_a\Big|^2 ds, \\ \zeta_3^2 &= \sum_{l\in\Gamma_i^h} h_l \int_l \Big|\alpha\frac{\partial u_h}{\partial n} + q_h\Big|^2 ds, \quad \zeta_4^2 = \sum_{l\in F^h} h_l \int_l [(\alpha\nabla u_h)\cdot n]^2 ds. \end{aligned} \tag{3.4}$$

To prove the main result of this section, we need the following lemma.

Lemma 3.4. *Let (u_h, p_h, q_h) be the solution of (2.6), and $u(q_h)$ and $p(q_h)$ be defined respectively by*

$$\big(\alpha\nabla u(q_h),\nabla\phi\big)+\big(ku(q_h),\phi\big)_{\Gamma_a}=(f,\phi)+(ku_a,\phi)_{\Gamma_a}-(q_h,\phi)_{\Gamma_i},\quad\forall\phi\in H^1(\Omega),\tag{3.5}$$

and

$$\big(\alpha\nabla p(q_h),\nabla\phi\big)+\big(kp(q_h),\phi\big)_{\Gamma_a}=\big(u(q_h)-z,\phi\big)_{\Gamma_a},\quad\forall\phi\in H^1(\Omega).\tag{3.6}$$

Then we have

$$\|p(q_h)-p_h\|_1^2\le C\bigg(\|u(q_h)-u_h\|_1^2+\sum_{i=1}^4\eta_i^2\bigg),\tag{3.7}$$

$$\|u(q_h)-u_h\|_1^2\le C\sum_{i=1}^4\zeta_i^2.\tag{3.8}$$

Proof. We first estimate the error $\|p(q_h)-p_h\|_1$. Let $e_p=p(q_h)-p_h$, $e_p^I=I_he_p$. Then applying the Poincaré inequality, (3.6) as well as the second equation in (2.6), and then integrating by parts in each element and applying the Cauchy-Schwartz inequality, we derive

$$\begin{aligned}
c\|e_p\|_1^2 &\le (\alpha\nabla e_p,\nabla e_p)+(ke_p,e_p)_{\Gamma_a}\\
&= \big(\alpha\nabla p(q_h)-\alpha\nabla p_h,\nabla e_p\big)+\big(kp(q_h)-kp_h,e_p\big)_{\Gamma_a}\\
&= \big(u(q_h)-z,e_p\big)_{\Gamma_a}-(\alpha\nabla p_h,\nabla e_p)-(kp_h,e_p)_{\Gamma_a}\\
&= \big(u(q_h)-u_h,e_p\big)_{\Gamma_a}+(u_h-z,e_p-e_p^I)_{\Gamma_a}+(u_h-z,e_p^I)_{\Gamma_a}\\
&\quad -(\alpha\nabla p_h,\nabla e_p)-(kp_h,e_p)_{\Gamma_a}\\
&= \big(u(q_h)-u_h,e_p\big)_{\Gamma_a}+(u_h-z,e_p-e_p^I)_{\Gamma_a}\\
&\quad -\big(\alpha\nabla p_h,\nabla(e_p-e_p^I)\big)-(kp_h,e_p-e_p^I)_{\Gamma_a}\\
&= \big(u(q_h)-u_h,e_p\big)_{\Gamma_a}+\sum_{l\in\Gamma_a^h}\int_l(u_h-z-kp_h-\alpha\frac{\partial p_h}{\partial n})(e_p-e_p^I)\\
&\quad +\sum_{\tau\in T^h}\int_\tau\big(\nabla\cdot(\alpha\nabla p_h)\big)(e_p-e_p^I)-\sum_{l\in F^h}\int_l[(\alpha\nabla p_h)\cdot n](e_p-e_p^I)\\
&\quad +\sum_{l\in\Gamma_i^h}\int_l\alpha\frac{\partial p_h}{\partial n}(e_p-e_p^I)\\
&\le \delta\|e_p\|_1^2+C_\delta\|u(q_h)-u_h\|_1^2+\delta\sum_{\tau\in T^h}h_\tau^{-2}\|e_p-e_p^I\|_{0,\tau}^2\\
&\quad +\delta\sum_{l\in\partial T^h}h_l^{-1}\|e_p-e_p^I\|_{0,l}^2+C_\delta(\eta_1^2+\eta_2^2+\eta_3^2+\eta_4^2)\\
&\le C\delta\|e_p\|_1^2+C_\delta\|u(q_h)-u_h\|_1^2+C_\delta(\eta_1^2+\eta_2^2+\eta_3^2+\eta_4^2),
\end{aligned}\tag{3.9}$$

where we have used the inequalities (3.1) and (3.3) in the second inequality. Taking δ small enough, we obtain the desired estimate (3.7) from (3.9).

Next, we estimate $\|u(q_h)-u_h\|_1$. Let $e_u=u(q_h)-u_h$, $e_u^I=I_he_u$. Analogously, by employing the Poincaré inequality, (3.5), the first equation in (2.6), integration by parts over each element and the

Cauchy-Schwartz inequality, we obtain,

$$\begin{aligned}
c\|e_u\|_1^2 &\le (\alpha\nabla e_u,\nabla e_u)+(ke_u,e_u)_{\Gamma_a}\\
&= (f,e_u)+(ku_a,e_u)_{\Gamma_a}-(q_h,e_u)_{\Gamma_i}\\
&\quad -(\alpha\nabla u_h,\nabla e_u)-(ku_h,e_u)_{\Gamma_a}\\
&= (f,e_u-e_u^I)+(ku_a,e_u-e_u^I)_{\Gamma_a}-(q_h,e_u-e_u^I)_{\Gamma_i}\\
&\quad -\big(\alpha\nabla u_h,\nabla(e_u-e_u^I)\big)-(ku_h,e_u-e_u^I)_{\Gamma_a}\\
&= \sum_{\tau\in T^h}\int_\tau\big(\nabla\cdot(\alpha\nabla u_h)+f\big)(e_u-e_u^I)-\sum_{l\in\Gamma_a^h}\int_l(\alpha\frac{\partial u_h}{\partial n}+ku_h-ku_a)(e_u-e_u^I) \qquad (3.10)\\
&\quad -\sum_{l\in\Gamma_i^h}\int_l(\alpha\frac{\partial u_h}{\partial n}+q_h)(e_u-e_u^I)+\sum_{l\in F^h}\int_l[(\alpha\nabla u_h)\cdot n](e_u-e_u^I)\\
&\le \delta\sum_{\tau\in T^h}h_\tau^{-2}\|e_u-e_u^I\|_{0,\tau}^2+\delta\sum_{l\in\partial T^h}h_l^{-1}\|e_u-e_u^I\|_{0,l}^2+C_\delta(\zeta_1^2+\zeta_2^2+\zeta_3^2+\zeta_4^2).
\end{aligned}$$

Now (3.8) follows by using (3.1) and (3.3) in the last inequality and taking δ small enough. □

With Lemma 3.4, we can now establish a posteriori error estimates in L^2-H^1 norm.

Theorem 3.5. *Let (u,p,q) and (u_h,p_h,q_h) be the solutions of (2.3) and (2.6), respectively. Then*

$$\|q-q_h\|_{0,\Gamma_i}^2+\|u-u_h\|_1^2+\|p-p_h\|_1^2 \le C\beta^{-2}\Big(\sum_{i=1}^4\eta_i^2+\sum_{i=1}^4\zeta_i^2\Big), \qquad (3.11)$$

where η_i,ζ_i $(1\le i\le 4)$ are defined in (3.4).

Proof. We first estimate the error $q-q_h$. For this, we note that the third equations in (2.3) and (2.6) imply respectively

$$\beta q=p\big|_{\Gamma_i},\quad \beta q_h=p_h\big|_{\Gamma_i}. \qquad (3.12)$$

It follows from (2.3), (3.5) and (3.6) that

$$(\alpha\nabla\big(u(q_h)-u\big),\nabla\phi)+(k\big(u(q_h)-u\big),\phi)_{\Gamma_a}=(q-q_h,\phi)_{\Gamma_i},\quad \forall\phi\in H^1(\Omega) \qquad (3.13)$$

and

$$(\alpha\nabla\big(p(q_h)-p\big),\nabla\phi)+(k\big(p(q_h)-p\big),\phi)_{\Gamma_a}=(u(q_h)-u,\phi)_{\Gamma_a},\quad \forall\phi\in H^1(\Omega). \qquad (3.14)$$

Taking $\phi=p(q_h)-p$ in (3.13) and $\phi=u(q_h)-u$ in (3.14), we know

$$\|u(q_h)-u\|_{0,\Gamma_a}^2=(q-q_h,p(q_h)-p)_{\Gamma_i},$$

noting (3.12) we have

$$\begin{aligned}
\beta\|q-q_h\|_{0,\Gamma_i}^2+\|u(q_h)-u\|_{0,\Gamma_a}^2 &= (q-q_h,\beta q-\beta q_h+p(q_h)-p)_{\Gamma_i}=(q-q_h,p(q_h)-p_h)_{\Gamma_i}\\
&\le \|q-q_h\|_{0,\Gamma_i}\cdot\|p(q_h)-p_h\|_{0,\Gamma_i},
\end{aligned}$$

which implies

$$\|q-q_h\|_{0,\Gamma_i}^2\le\beta^{-2}\|p(q_h)-p_h\|_{0,\Gamma_i}^2. \qquad (3.15)$$

Now combining (3.15) with (3.7) and (3.8) yields

$$\|q_h-q\|_{0,\Gamma_i}^2\le C\beta^{-2}\Big(\sum_{i=1}^4\eta_i^2+\sum_{i=1}^4\zeta_i^2\Big). \qquad (3.16)$$

We continue with estimating the errors for the state and costate variables. First, putting $\phi=u(q_h)-u$ in (3.13) and applying the Poincaré inequality and the trace theorem, we deduce

$$\|u(q_h)-u\|_1^2\le C\|q-q_h\|_{0,\Gamma_i}\|u(q_h)-u\|_1,$$

which implies

$$\|u(q_h) - u\|_1 \leq C\|q - q_h\|_{0,\Gamma_i}. \tag{3.17}$$

It is easy to see from (3.8), (3.17) and the triangle inequality that

$$\|u_h - u\|_1^2 \leq C\beta^{-2}\Big(\sum_{i=1}^4 \eta_i^2 + \sum_{i=1}^4 \zeta_i^2\Big). \tag{3.18}$$

Similarly, by taking $\phi = p(q_h) - p$ in (3.14) and applying the Poincaré and Cauchy-Schwartz inequalities, we derive

$$\|p(q_h) - p\|_1 \leq C\|u(q_h) - u\|_1. \tag{3.19}$$

It follows readily from (3.7), (3.17), and (3.18) that

$$\|p_h - p\|_1^2 \leq C\beta^{-2}\Big(\sum_{i=1}^4 \eta_i^2 + \sum_{i=1}^4 \zeta_i^2\Big), \tag{3.20}$$

which completes the proof of the desired estimate (3.11). □

Remark 3.6. It is observed that the error terms η_i's are contributions from the approximation errors of the costate variable respectively in Ω, Γ_a, and Γ_i (noting that homogeneous Neumann boundary condition is imposed for p on Γ_i, see the second equation in (2.3) or (2.6)). The error terms ζ_i's are contributions from the approximation errors of the state variable respectively in Ω, Γ_a, and Γ_i. The local error estimators used for our numerical experiments is always obtained by summing over all the local contributions of η_i's and ζ_i's associated with a local element and all its faces.

Remark 3.7. It is important to note that factor β^{-2} enters the upper bound explicitly in (3.11). This explicit dependence seems to indicate that factor β^{-2} plays an amplification role. But we have observed from many numerical experiments (see some examples in Section 4), the efficiency of the a posteriori error estimator remains up to a scaling effect. More importantly, the error estimators indicate the correct locations for local refinements by relative magnitude of the a posteriori error estimates regardless of the amplification factor β^{-2}.

3.2 Lower error bounds

In this subsection, we shall establish the lower error bound, which demonstrates that the error estimates obtained in Section 3.1 are optimal up to a scaling in some sense. We start with the following lemma about bubble functions, whose proof can be found in [1, 19].

Lemma 3.8. *Let $\tau \in T^h$. For any $l \in F^h$, let τ_l^1, τ_l^2 be two elements in T^h sharing the common face l. For any $l \in \Gamma^h$, let τ_l be the element having l as one of its faces. Then for any constants A_τ, B_l, and B_f, there exist polynomials $w_\tau \in H_0^1(\tau)$, $w_l \in H_0^1(\tau_l^1 \cup \tau_l^2)$, and $w_f \in \{w \in H^1(\tau_l) : w = 0 \text{ on } \partial\tau_l \setminus l\}$ such that, for $m = 0, 1$ and all $\tau \in T^h$ and $l \in F^h$,*

$$\int_\tau A_\tau w_\tau dx = h_\tau^2 \int_\tau A_\tau^2 dx, \quad |w_\tau|_{m,\tau}^2 \leq C h_\tau^{2(1-m)+2} \int_\tau A_\tau^2 dx, \tag{3.21}$$

$$\int_l B_l w_l ds = h_l \int_l B_l^2 ds, \quad |w_l|_{m,\tau_l^1 \cup \tau_l^2}^2 \leq C h_l^{2(1-m)+1} \int_l B_l^2 ds, \tag{3.22}$$

$$\int_l B_f w_f ds = h_l \int_l B_f^2 ds, \quad |w_f|_{m,\tau_l}^2 \leq C h_l^{2(1-m)+1} \int_l B_f^2 ds. \tag{3.23}$$

We introduce the following a posteriori quantities:

$$F_1 = \nabla\cdot(\alpha\nabla p_h), \quad F_2 = \alpha\frac{\partial p_h}{\partial n} + kp_h - (u_h - z), \quad F_3 = \alpha\frac{\partial p_h}{\partial n}, \quad F_4 = [(\alpha\nabla p_h)\cdot n],$$
$$G_1 = \nabla\cdot(\alpha\nabla u_h) + f, \quad G_2 = \alpha\frac{\partial u_h}{\partial n} + ku_h - ku_a, \quad G_3 = \alpha\frac{\partial u_h}{\partial n} + q_h, \quad G_4 = [(\alpha\nabla u_h)\cdot n].$$

For any domain D and function $F \in L^2(D)$, we define its average as

$$\bar{F}|_D = \frac{1}{|D|}\int_D F dx. \tag{3.24}$$

It follows from the Cauchy-Schwartz inequality that

$$\int_D \bar{F}^2 dx \le \int_D F^2 dx.$$

Theorem 3.9. *Let (u,p,q) and (u_h,p_h,q_h) be the solutions of (2.3) and (2.6), respectively. Then*

$$\begin{aligned}\sum_{i=1}^4(\eta_i^2+\zeta_i^2) \;\le\;& C(\|q-q_h\|^2_{0,\Gamma_i} + \|u-u_h\|_1^2 + \|p-p_h\|_1^2)\\ &+C\sum_{\tau\in T^h} h_\tau^2(\|F_1-\bar{F}_1\|^2_{0,\tau} + \|G_1-\bar{G}_1\|^2_{0,\tau})\\ &+C\sum_{l\in\Gamma_a^h} h_l(\|F_2-\bar{F}_2\|^2_{0,l} + \|G_2-\bar{G}_2\|^2_{0,l})\\ &+C\sum_{l\in\Gamma_i^h} h_l(\|F_3-\bar{F}_3\|^2_{0,l} + \|G_3-\bar{G}_3\|^2_{0,l})\\ &+C\sum_{l\in F^h} h_l(\|F_4-\bar{F}_4\|^2_{0,l} + \|G_4-\bar{G}_4\|^2_{0,l}),\end{aligned}$$

where η_i, ζ_i $(1\le i\le 4)$ are defined in (3.4), and the quantities with a bar are the average of the corresponding quantities in the associated elements or faces.

Proof. We demonstrate only how to bound the terms in η_i^2, while similar estimates can be applied to the terms in ζ_i^2. We first estimate η_1^2. Let w_τ be the bubble function as in Lemma 3.8 with $A_\tau = \bar{F}_1|_\tau$ for any element $\tau\in T^h$. Then we deduce

$$\begin{aligned}\eta_1^2 &= \sum_{\tau\in T^h} h_\tau^2\int_\tau F_1^2 \le 2\sum_{\tau\in T^h} h_\tau^2\int_\tau\big(\bar{F}_1^2 + (F_1-\bar{F}_1)^2\big)\\ &= 2\sum_{\tau\in T^h}\int_\tau\big(w_\tau F_1 + w_\tau(\bar{F}_1-F_1) + h_\tau^2(F_1-\bar{F}_1)^2\big)\\ &= 2\sum_{\tau\in T^h}\int_\tau\Big\{-\alpha\nabla p_h\cdot\nabla w_\tau + w_\tau(\bar{F}_1-F_1) + h_\tau^2(F_1-\bar{F}_1)^2\Big\}\\ &= 2\sum_{\tau\in T^h}\int_\tau\Big\{-\alpha\nabla p(q_h)\cdot\nabla w_\tau + \alpha\nabla\big(p(q_h)-p_h\big)\cdot\nabla w_\tau\\ &\quad + w_\tau(\bar{F}_1-F_1) + h_\tau^2(F_1-\bar{F}_1)^2\Big\}.\end{aligned}$$

Using equation (3.6) and Lemma 3.8, we obtain

$$\begin{aligned}\eta_1^2 &\le C\sum_{\tau\in T^h}\big|p(q_h)-p_h\big|^2_{1,\tau} + \delta\sum_{\tau\in T^h}\big(|w_\tau|^2_{1,\tau} + h_\tau^{-2}\|w_\tau\|^2_{0,\tau}\big) + C\sum_{\tau\in T^h} h_\tau^2\int_\tau(F_1-\bar{F}_1)^2\\ &\le C\big(\|p(q_h)-p\|_1^2 + \|p-p_h\|_1^2\big) + C\delta\eta_1^2 + C\sum_{\tau\in T^h} h_\tau^2\int_\tau(F_1-\bar{F}_1)^2.\end{aligned}$$

Taking δ small enough, it follows from (3.17) and (3.19) that

$$\eta_1^2 \le C\big(\|p_h - p\|_1^2 + \|q - q_h\|_{0,\Gamma_i}^2\big) + C\sum_{\tau\in T^h} h_\tau^2 \|F_1 - \bar{F}_1\|_{0,\tau}^2. \tag{3.25}$$

Next, we bound η_2^2. Let w_f be the bubble function as in Lemma 3.8 with $B_f = \bar{F}_2|_l$ for any face $l \in \Gamma_a^h$. Then we deduce

$$\begin{aligned}
\eta_2^2 &= \sum_{l\in\Gamma_a^h} h_l \int_l F_2^2 \le 2\sum_{l\in\Gamma_a^h} h_l \int_l \big(\bar{F}_2^2 + (F_2 - \bar{F}_2)^2\big) \\
&= 2\sum_{l\in\Gamma_a^h} \int_l \big(w_f F_2 + w_f(\bar{F}_2 - F_2) + h_l(F_2 - \bar{F}_2)^2\big) \\
&= 2\sum_{l\in\Gamma_a^h} \Big\{ \int_{\tau_l} \big(\nabla\cdot(\alpha\nabla p_h)w_f + \alpha\nabla p_h\cdot\nabla w_f\big) \\
&\quad + \int_l \big((kp_h - u_h + z)w_f + w_f(\bar{F}_2 - F_2) + h_l(F_2 - \bar{F}_2)^2\big)\Big\} \\
&= 2\sum_{l\in\Gamma_a^h} \Big\{ \int_{\tau_l} \big\{\nabla\cdot(\alpha\nabla p_h)w_f + \alpha\nabla p(q_h)\cdot\nabla w_f + \alpha\nabla\big(p_h - p(q_h)\big)\cdot\nabla w_f\big\} \\
&\quad + \int_l \big((kp_h - u_h + z)w_f + w_f(\bar{F}_2 - F_2) + h_l(F_2 - \bar{F}_2)^2\big)\Big\}.
\end{aligned}$$

Using equations (3.6), (3.3), and Lemma 3.8, we have

$$\begin{aligned}
\eta_2^2 &= 2\sum_{l\in\Gamma_a^h} \Big\{ \int_{\tau_l} \big\{\nabla\cdot(\alpha\nabla p_h)w_f + \alpha\nabla\big(p_h - p(q_h)\big)\cdot\nabla w_f\big\} \\
&\quad + \int_l \big\{k\big(p_h - p(q_h)\big)w_f + \big(u(q_h) - u_h\big)w_f + w_f(\bar{F}_2 - F_2) + h_l(F_2 - \bar{F}_2)^2\big\}\Big\} \\
&\le C\eta_1^2 + \delta\sum_{l\in\Gamma_a^h} (h_l^{-2}\|w_f\|_{0,\tau_l}^2 + |w_f|_{1,\tau_l}^2) + C\sum_{l\in\Gamma_a^h} h_l\|u(q_h) - u_h\|_{1,\tau_l}^2 \\
&\quad + C\sum_{l\in\Gamma_a^h} \|p_h - p(q_h)\|_{1,\tau_l}^2 + \delta\sum_{l\in\Gamma_a^h} h_l^{-1}\|w_f\|_{0,l}^2 + C\sum_{l\in\Gamma_a^h}\int_l h_l(F_2 - \bar{F}_2)^2 \\
&\le C\eta_1^2 + C\delta\eta_2^2 + C\sum_{l\in\Gamma_a^h}\int_l h_l(F_2 - \bar{F}_2)^2 + C(\|p_h - p(q_h)\|_1^2 + h\|u(q_h) - u_h\|_1^2).
\end{aligned}$$

Similarly to the derivation of (3.25), taking δ small enough, we obtain

$$\begin{aligned}
\eta_2^2 \le\ & C\big(\|p_h - p\|_1^2 + h\|u - u_h\|_1^2 + \|q - q_h\|_{0,\Gamma_i}^2\big) \\
& + C\sum_{\tau\in T^h} h_\tau^2\|F_1 - \bar{F}_1\|_{0,\tau}^2 + C\sum_{l\in\Gamma_a^h} h_l\|F_2 - \bar{F}_2\|_{0,l}^2.
\end{aligned} \tag{3.26}$$

To bound η_3^2, let w_f be the bubble function as in Lemma 3.8 with $B_f = \bar{F}_3|_l$ for any face $l \in \Gamma_i^h$.

Then we deduce similarly as it was done for η_2 above

$$\begin{aligned}
\eta_3^2 &\le 2\sum_{l\in\Gamma_i^h}\int_l \big(w_f F_3 + w_f(\bar F_3 - F_3) + h_l(F_3-\bar F_3)^2\big)\\
&= 2\sum_{l\in\Gamma_i^h}\Big\{\int_{\tau_l}\big(\nabla\cdot(\alpha\nabla p_h)w_f + \alpha\nabla p_h\cdot\nabla w_f\big) + \int_l\big(w_f(\bar F_3 - F_3) + h_l(F_3-\bar F_3)^2\big)\Big\}\\
&= 2\sum_{l\in\Gamma_i^h}\Big\{\int_{\tau_l}\big\{\nabla\cdot(\alpha\nabla p_h)w_f + \alpha\nabla p(q_h)\cdot\nabla w_f + \alpha\nabla\big(p_h - p(q_h)\big)\cdot\nabla w_f\big\}\\
&\quad + \int_l\big(w_f(\bar F_3 - F_3) + h_l(F_3-\bar F_3)^2\big)\Big\}.
\end{aligned}$$

Using equations (3.6), (3.3), and Lemma 3.8, we come to

$$\begin{aligned}
\eta_3^2 &= 2\sum_{l\in\Gamma_i^h}\Big\{\int_{\tau_l}\big\{\nabla\cdot(\alpha\nabla p_h)w_f + \alpha\nabla\big(p_h - p(q_h)\big)\cdot\nabla w_f\big\}\\
&\quad + \int_l\big(w_f(\bar F_3 - F_3) + h_l(F_3-\bar F_3)^2\big)\Big\}\\
&\le C\eta_1^2 + \delta\sum_{l\in\Gamma_i^h}(h_l^{-2}\|w_f\|_{0,\tau_l}^2 + |w_f|_{1,\tau_l}^2) + C\sum_{l\in\Gamma_i^h}|p_h - p(q_h)|_{1,\tau_l}^2\\
&\quad + \delta\sum_{l\in\Gamma_i^h}h_l^{-1}\|w_f\|_{0,l}^2 + C\sum_{l\in\Gamma_i^h}\int_l h_l(F_3-\bar F_3)^2\\
&\le C\eta_1^2 + C\delta\eta_3^2 + C\sum_{l\in\Gamma_i^h}\int_l h_l(F_3-\bar F_3)^2 + C\|p_h - p(q_h)\|_1^2,
\end{aligned}$$

which implies

$$\eta_3^2 \le C\big(\|p_h - p\|_1^2 + \|q - q_h\|_{0,\Gamma_i}^2\big) + C\sum_{\tau\in T^h}h_\tau^2\|F_1 - \bar F_1\|_{0,\tau}^2 + C\sum_{l\in\Gamma_i^h}h_l\|F_3 - \bar F_3\|_{0,l}^2. \tag{3.27}$$

To bound η_4^2, let w_l be the bubble function as in Lemma 3.8 with $B_l = \bar F_4|_l$ for any interior face $l \in F^h$. Then we can deduce similarly as it was done for η_2 above

$$\begin{aligned}
\eta_4^2 &\le 2\sum_{l\in F^h}\int_l \big(w_l F_4 + w_l(\bar F_4 - F_4) + h_l(F_4-\bar F_4)^2\big)\\
&= 2\sum_{l\in F^h}\Big\{\int_{\tau_l^1\cup\tau_l^2}\big(\nabla\cdot(\alpha\nabla p_h)w_l + \alpha\nabla p_h\cdot\nabla w_l\big) + \int_l\big(w_l(\bar F_4 - F_4) + h_l(F_4-\bar F_4)^2\big)\Big\}\\
&= 2\sum_{l\in F^h}\Big\{\int_{\tau_l^1\cup\tau_l^2}\big\{\nabla\cdot(\alpha\nabla p_h)w_l + \alpha\nabla p(q_h)\cdot\nabla w_l + \alpha\nabla\big(p_h - p(q_h)\big)\cdot\nabla w_l\big\}\\
&\quad + \int_l\big(w_l(\bar F_4 - F_4) + h_l(F_4-\bar F_4)^2\big)\Big\}.
\end{aligned}$$

It follows from (3.6), (3.3), and Lemma 3.8 that

$$\begin{aligned}
\eta_4^2 &= 2\sum_{l\in F^h}\Big\{\int_{\tau_l^1\cup\tau_l^2}\big\{\nabla\cdot(\alpha\nabla p_h)w_l+\alpha\nabla\big(p_h-p(q_h)\big)\cdot\nabla w_l\big\}\\
&\quad+\int_l\big(w_l(\bar F_4-F_4)+h_l(F_4-\bar F_4)^2\big)\Big\}\\
&\le C\eta_1^2+\delta\sum_{l\in F^h}(h_l^{-2}\|w_l\|^2_{0,\tau_l^1\cup\tau_l^2}+|w_l|^2_{1,\tau_l^1\cup\tau_l^2})\\
&\quad+C\sum_{l\in F^h}|p_h-p(q_h)|^2_{1,\tau_l^1\cup\tau_l^2}+\delta\sum_{l\in F^h}h_l^{-1}\|w_l\|^2_{0,l}+C\sum_{l\in\Gamma_i^h}\int_l h_l(F_4-\bar F_4)^2\\
&\le C\eta_1^2+C\delta\eta_4^2+C\sum_{l\in F^h}\int_l h_l(F_4-\bar F_4)^2+C\|p_h-p(q_h)\|_1^2,
\end{aligned}$$

or

$$\eta_4^2\le C\big(\|p_h-p\|_1^2+\|q-q_h\|^2_{0,\Gamma_i}\big)+C\sum_{\tau\in T^h}h_\tau^2\|F_1-\bar F_1\|^2_{0,\tau}+C\sum_{l\in F^h}h_l\|F_4-\bar F_4\|^2_{0,l}. \tag{3.28}$$

This completes the estimates of terms η_i^2. □

3.3 A posteriori estimates: L^2-L^2 norms

We have derived in the previous subsection the a posteriori error estimate for q in the L^2-norm, for u and p in the H^1-norm. In some applications, it may be more interesting to know the errors in the L^2-norm for both state and costate variables. This is the task of this section.

We first introduce the following a posteriori errors:

$$\begin{aligned}
\hat\eta_1^2 &= \sum_{\tau\in T^h}h_\tau^4\int_\tau|\nabla\cdot(\alpha\nabla p_h)|^2dx,\quad \hat\eta_2^2=\sum_{l\in\Gamma_a^h}h_l^3\int_l\Big|\alpha\frac{\partial p_h}{\partial n}+kp_h-u_h+z\Big|^2ds,\\
\hat\eta_3^2 &= \sum_{l\in\Gamma_i^h}h_l^3\int_l\Big|\alpha\frac{\partial p_h}{\partial n}\Big|^2ds,\quad \hat\eta_4^2=\sum_{l\in F^h}h_l^3\int_l[(\alpha\nabla p_h)\cdot n]^2ds,\\
\tilde\eta_1^2 &= \sum_{\tau\in T^h}h_\tau^3\int_\tau|\nabla\cdot(\alpha\nabla p_h)|^2dx,\quad \tilde\eta_2^2=\sum_{l\in\Gamma_a^h}h_l^2\int_l\Big|\alpha\frac{\partial p_h}{\partial n}+kp_h-u_h+z\Big|^2ds,\\
\tilde\eta_3^2 &= \sum_{l\in\Gamma_i^h}h_l^2\int_l\Big|\alpha\frac{\partial p_h}{\partial n}\Big|^2ds,\quad \tilde\eta_4^2=\sum_{l\in F^h}h_l^2\int_l[(\alpha\nabla p_h)\cdot n]^2ds,\\
\hat\zeta_1^2 &= \sum_{\tau\in T^h}h_\tau^4\int_\tau|f+\nabla\cdot(\alpha\nabla u_h)|^2dx,\quad \hat\zeta_2^2=\sum_{l\in\Gamma_a^h}h_l^3\int_l\Big|\alpha\frac{\partial u_h}{\partial n}+ku_h-ku_a\Big|^2ds,\\
\hat\zeta_3^2 &= \sum_{l\in\Gamma_i^h}h_l^3\int_l\Big|\alpha\frac{\partial u_h}{\partial n}+q_h\Big|^2ds,\quad \hat\zeta_4^2=\sum_{l\in F^h}h_l^3\int_l[(\alpha\nabla u_h)\cdot n]^2ds,\\
\tilde\zeta_1^2 &= \sum_{\tau\in T^h}h_\tau^3\int_\tau|f+\nabla\cdot(\alpha\nabla u_h)|^2dx,\quad \tilde\zeta_2^2=\sum_{l\in\Gamma_a^h}h_l^2\int_l\Big|\alpha\frac{\partial u_h}{\partial n}+ku_h-ku_a\Big|^2ds,\\
\tilde\zeta_3^2 &= \sum_{l\in\Gamma_i^h}h_l^2\int_l\Big|\alpha\frac{\partial u_h}{\partial n}+q_h\Big|^2ds,\quad \tilde\zeta_4^2=\sum_{l\in F^h}h_l^2\int_l[(\alpha\nabla u_h)\cdot n]^2ds.
\end{aligned}\tag{3.29}$$

then we can derive the following estimates.

Theorem 3.10. *Let (u,p,q) and (u_h,p_h,q_h) be the solutions of (2.3) and (2.6), respectively. Then*

$$\|q_h-q\|^2_{0,\Gamma_i}+\|p_h-p\|_0^2+\|u_h-u\|_0^2\le C\bigg(\sum_{i=1}^4\hat\eta_i^2+\sum_{i=1}^4\hat\zeta_i^2+\beta^{-2}\sum_{i=1}^4\tilde\eta_i^2+\beta^{-2}\sum_{i=1}^4\tilde\zeta_i^2\bigg). \tag{3.30}$$

Proof. The proof is accomplished by the dual argument. We divide the proof into five steps. In the first step we estimate $\|p(q_h) - p_h\|_{0,\Gamma_i}$. For this, we construct the first auxiliary problem: Find $\xi \in H^1(\Omega)$ such that

$$(\alpha\nabla\xi, \nabla\phi) + (k\xi, \phi)_{\Gamma_a} = (f_1, \phi)_{\Gamma_i}, \quad \forall \phi \in H^1(\Omega). \tag{3.31}$$

By the regularity of elliptic equations (see, e.g. [13]), we have

$$\|\xi\|_{\frac{3}{2}} \leq C\|f_1\|_{0,\Gamma_i}. \tag{3.32}$$

Take $f_1 = \big(p(q_h) - p_h\big)\big|_{\Gamma_i}$ in (3.31) and let $\xi^\pi = \pi_h\xi$ be the standard Lagrange interpolation of the corresponding solution ξ in V^h. It follows from (3.6) and the second equation in (2.6) that

$$\begin{aligned}
& \|p(q_h) - p_h\|^2_{0,\Gamma_i} = \big(f_1, p(q_h) - p_h\big)_{\Gamma_i} \\
= \;& \big(\alpha\nabla\xi, \nabla p(q_h)\big) + \big(k\xi, p(q_h)\big)_{\Gamma_a} - (\alpha\nabla\xi, \nabla p_h) - (k\xi, p_h)_{\Gamma_a} \\
= \;& \big(u(q_h) - z, \xi\big)_{\Gamma_a} - (u_h - z, \xi)_{\Gamma_a} - \big(\alpha\nabla(\xi - \xi^\pi), \nabla p_h\big) \\
& -\big(k(\xi - \xi^\pi), p_h\big)_{\Gamma_a} - (\alpha\nabla\xi^\pi, \nabla p_h) - (k\xi^\pi, p_h)_{\Gamma_a} + (u_h - z, \xi)_{\Gamma_a} \\
= \;& \big(u(q_h) - u_h, \xi\big)_{\Gamma_a} - \big(\alpha\nabla(\xi - \xi^\pi), \nabla p_h\big) - \big(k(\xi - \xi^\pi), p_h\big)_{\Gamma_a} + (u_h - z, \xi - \xi^\pi) \\
= \;& \big(u(q_h) - u_h, \xi\big)_{\Gamma_a} - \big(\alpha\nabla p_h, \nabla(\xi - \xi^\pi)\big) - \big(kp_h, \xi - \xi^\pi\big)_{\Gamma_a} + (u_h - z, \xi - \xi^\pi).
\end{aligned}$$

Integrating by parts in each element and applying the Cauchy-Schwartz inequality, we obtain

$$\begin{aligned}
\|p(q_h) - p_h\|^2_{0,\Gamma_i} \;\leq\; & \delta\|\xi\|^2_{0,\Gamma_a} + C_\delta\|u(q_h) - u_h\|^2_{0,\Gamma_a} + \delta\sum_{\tau\in T^h} h_\tau^{-3}\|\xi - \xi^\pi\|^2_{0,\tau} + C\tilde{\eta}_1^2 \\
& +\delta\sum_{l\in\partial T^h} h_l^{-2}\|\xi - \xi^\pi\|^2_{0,l} + C(\tilde{\eta}_2^2 + \tilde{\eta}_3^2 + \tilde{\eta}_4^2).
\end{aligned}$$

It follows from equations (3.2), (3.3), and the Sobolev interpolation inequality that

$$\sum_{\tau\in T^h} h_\tau^{-3}\|\xi - \xi^\pi\|^2_{0,\tau} \leq C\|\xi\|^2_{\frac{3}{2}}, \qquad \sum_{l\in\partial T^h} h_l^{-2}\|\xi - \xi^\pi\|^2_{0,l} \leq C\|\xi\|^2_{\frac{3}{2}}.$$

Taking δ small enough and using (3.32) we obtain

$$\|p(q_h) - p_h\|^2_{0,\Gamma_i} \leq C\bigg(\|u(q_h) - u_h\|^2_{0,\Gamma_a} + \sum_{i=1}^4 \tilde{\eta}_i^2\bigg). \tag{3.33}$$

In the second step, we aim at estimating $\|u(q_h) - u_h\|_{0,\Gamma_a}$. For this, we construct the second auxiliary problem: Find $\xi \in H^1(\Omega)$ such that

$$(\alpha\nabla\xi, \nabla\phi) + (k\xi, \phi)_{\Gamma_a} = (f_2, \phi)_{\Gamma_a}, \quad \forall \phi \in H^1(\Omega). \tag{3.34}$$

Taking $f_2 = \big(u(q_h) - u_h\big)\big|_{\Gamma_a}$ in (3.34), it follows from the same trick as above that

$$\|u(q_h) - u_h\|^2_{0,\Gamma_a} \leq C\sum_{i=1}^4 \tilde{\zeta}_i^2. \tag{3.35}$$

Plugging (3.35) into (3.33) and using (3.15), we obtain

$$\|q_h - q\|^2_{0,\Gamma_i} \leq C\beta^{-2}\big(\sum_{i=1}^4 \tilde{\eta}_i^2 + \sum_{i=1}^4 \tilde{\zeta}_i^2\big). \tag{3.36}$$

In the third step, we estimate $\|u(q_h) - u_h\|_0$. To achieve this, we construct the third auxiliary problem as: Find $\upsilon \in H^1(\Omega)$ such that

$$(\alpha\nabla\upsilon, \nabla\phi) + (k\upsilon, \phi)_{\Gamma_a} = (f_3, \phi), \quad \forall\phi \in H^1(\Omega). \tag{3.37}$$

By the regularity of elliptic equations, we have

$$\|\upsilon\|_2 \le C\|f_3\|_0. \tag{3.38}$$

Taking $f_3 = u(q_h) - u_h$ in (3.37), it follows from (3.5) and the first equation in (2.6) that

$$\begin{aligned}
& \|u(q_h) - u_h\|_0^2 = \big(f_3, u(q_h) - u_h\big) \\
= \;& \big(\alpha\nabla\upsilon, \nabla u(q_h)\big) + \big(k\upsilon, u(q_h)\big)_{\Gamma_a} - (\alpha\nabla\upsilon, \nabla u_h) - (k\upsilon, u_h)_{\Gamma_a} \\
= \;& (f, \upsilon) + (ku_a, \upsilon)_{\Gamma_a} - (q_h, \upsilon)_{\Gamma_i} - \big(\alpha\nabla u_h, \nabla(\upsilon - \upsilon^\pi)\big) \\
& -\big(ku_h, \upsilon - \upsilon^\pi\big)_{\Gamma_a} - (\alpha\nabla u_h, \nabla\upsilon^\pi) - (ku_h, \upsilon^\pi)_{\Gamma_a} \\
= \;& (f, \upsilon - \upsilon^\pi) + (ku_a, \upsilon - \upsilon^\pi)_{\Gamma_a} - (q_h, \upsilon - \upsilon^\pi)_{\Gamma_i} \\
& -\big(\alpha\nabla u_h, \nabla(\upsilon - \upsilon^\pi)\big) - \big(ku_h, \upsilon - \upsilon^\pi\big)_{\Gamma_a},
\end{aligned}$$

where $\upsilon^\pi = \pi_h\upsilon$. Integrating by parts in each element and applying the Cauchy-Schwartz inequality, and equations (3.2)-(3.3), we obtain

$$\begin{aligned}
\|u(q_h) - u_h\|_0^2 \;\le\; & \delta \sum_{\tau\in T^h} h_\tau^{-4}\|\upsilon - \upsilon^\pi\|_{0,\tau}^2 + C\hat{\zeta}_1^2 \\
& +\delta \sum_{l\in\partial T^h} h_l^{-3}\|\upsilon - \upsilon^\pi\|_{0,l}^2 + C(\hat{\zeta}_2^2 + \hat{\zeta}_3^2 + \hat{\zeta}_4^2) \\
\le \;& C\delta\|\upsilon\|_2^2 + C\sum_{i=1}^4 \hat{\zeta}_i^2.
\end{aligned}$$

It then follows from (3.38) by taking δ small enough that

$$\|u(q_h) - u_h\|_0^2 \le C\sum_{i=1}^4 \hat{\zeta}_i^2. \tag{3.39}$$

In the fourth step we estimate $\|p(q_h) - p_h\|_0$. To do this, we use the third auxiliary problem (3.37) again, but taking $f_3 = p(q_h) - p_h$ this time. The corresponding solution to (3.37) is now denoted by ν. Then it follows from the elliptic regularity that

$$\|\nu\|_2 \le C\|p(q_h) - p_h\|_0. \tag{3.40}$$

Using the same argument as before, we obtain

$$\begin{aligned}
\|p(q_h) - p_h\|_0^2 \;\le\; & \delta \sum_{\tau\in T^h} h_\tau^{-4}\|\nu - \nu^\pi\|_{0,\tau}^2 + \delta \sum_{l\in\partial T^h} h_l^{-3}\|\nu - \nu^\pi\|_{0,l}^2 + C\sum_{i=1}^4 \hat{\eta}_i^2 \\
& +\delta\|\nu\|_0^2 + C\|u(q_h) - u_h\|_{0,\Gamma_a}^2 \\
\le \;& C\delta\|\nu\|_2^2 + C\sum_{i=1}^4 \hat{\eta}_i^2 + C\|u(q_h) - u_h\|_{0,\Gamma_a}^2.
\end{aligned}$$

Consequently, by taking δ small enough, equation (3.40) together with (3.35) implies

$$\|p(q_h) - p_h\|_0^2 \le C\bigg(\sum_{i=1}^4 \hat{\eta}_i^2 + \sum_{i=1}^4 \tilde{\zeta}_i^2\bigg). \tag{3.41}$$

Now the desired estimates in Theorem 3.10 follow readily from the triangle inequality and (3.17), (3.19), (3.36). □

4 Numerical Experiments and discussions

In this section, we present some numerical experiments to validate the applicability and efficiency of the error estimators derived in the previous sections. Throughout the spatial discretization is always done with continuous piecewise linear finite elements on triangles. The resulting nonlinear discrete optimality system (2.6) is solved by the damped Newton method, whereas the linear subproblems in (2.6) are treated by fast direct solvers in the UMFPACK library. All the computations are done with Matlab on a four-core desktop with AMD 925 processors and 16GB memory.

We will mainly focus on the difficulties arising from the challenging nature of different types of distributed heat fluxes. To make our examples more practical and reasonable, the true solution of the stationary heat conductive equation (2.1) is assumed to be unknown in advance and is calculated in an extremely fine mesh. In real inverse problems, the boundary data is experimentally measured and thus inevitably contaminated by measurement errors. In our examples, the simulated noisy data is synthesized as follows:

$$z(x) = u(x) + \delta \cdot u(x) rand(x)$$

where $u(x)$ denotes the true solution, δ represents the noise level and $rand(x)$ is a nodal-wise uniformly random number between -1 and 1. For the reconstruction of distributed heat flux, we always set $\alpha = 1$, $k = 1$, $u_a = 0$ and $f = 0$. The noise level δ is always chosen to be 1% and the initial guess of the unknown flux is always set to zero everywhere. The element selection method uses the Babuska-Rheinboldt strategy [3], i.e., triangles are selected for refinement when its local error estimator exceeds a fraction (0.5 here) of the worst estimator among all the elements. For ease of visualization, the inner boundary plot is parametrized in the order of left, bottom, right and top by its arc length so that the heat flux can be represented by a function of arc length.

Example 1. (Discontinuous heat flux) The computational domain is a well-shaped region $\Omega = (-1,1)\times(-1,1)\backslash(-0.6,0.6)\times(-0.6,0.6)$. The accessible part consists of all the outer boundaries while all the inner boundaries are inaccessible. The true heat flux is discontinuous at the points $(-0.6, 0.6)$ and $(0.6, 0.6)$ and given by

$$q(x,y) = \begin{cases} 1 & \text{if } x = 0.6,\ -0.6 < y < 0.6, \\ 0 & \text{if } x = -0.6,\ -0.6 < y < 0.6, \\ 0 & \text{if } y = 0.6,\ -0.6 < x < 0.6, \\ 0 & \text{if } y = -0.6,\ -0.6 < x < 0.6, \end{cases}$$

and the true solution u and the initial mesh are shown in Figure 1(a) and (b), respectively. This example is highly non-trivial due to the fact that the heat flux q is discontinuous on the right two reentrant corners $(-0.6, 0.6)$ and $(0.6, 0.6)$.

First, we investigate the numerical flux reconstruction by using the $L^2 - H^1$ error estimator. Figure 2 shows the reconstructed flux and some intermediate meshes after 10 adaptive refinements. The error estimator is able to locate approximately where the discontinuity lies such that the adaptive refinement is guided to be done mainly around the two corners $(-0.6, 0.6)$ and $(0.6, 0.6)$ in a progressive way. It can be observed that the reconstructed heat flux resembles quite well the original piecewise constant true one except some small oscillation around the corners with the flux discontinuity. Such oscillating phenomena are essential for the heat flux reconstruction. As is well known, the distributed heat flux reconstruction problem is much more difficult to solve than the direct problem in which the boundary conditions are given and the temperature is to be determined. In the direct problem the high frequency modes of the heat fluxes are damped out due to the diffusion nature of the heat conduction process. This makes it extremely difficult numerically for the heat flux reconstruction using the temperature measurement. And the high frequency modes or noise in the temperature measurements on the accessible boundaries will be amplified in the projection to the inaccessible boundaries and lead to oscillations in the numerical surface fluxes. The regularization parameter

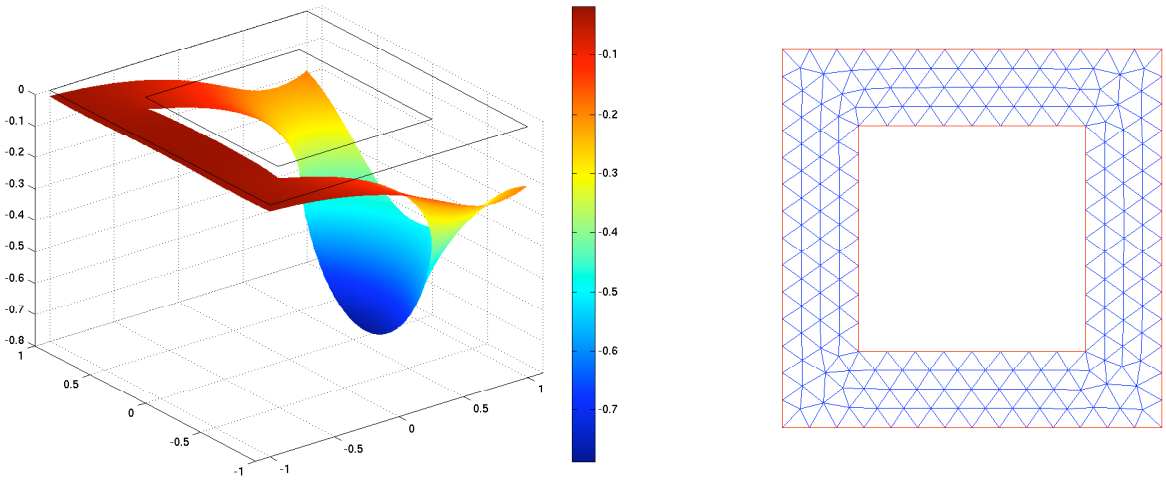

(a) (b)

Figure 1: True solution u (a) and the initial mesh (b) with 448 dofs in Example 1.

plays a key role to suppress the oscillation. However, over-estimated regularization parameters may introduce an undesirable side-effect that sharp jumps could be smeared off.

Next, we repeat the test under the same setting by using the $L^2 - L^2$ error estimator for 10 adaptive refinements. Like the $L^2 - H^1$ case, as we can see, adaptive meshes cluster gradually around the singular corners $(-0.6, 0.6)$ and $(0.6, 0.6)$ as shown in Figure 3(b), (c) and (d), which enables us to approximate well the sharp jumps in the discontinuous profile of the true heat flux around the singular points as shown in Figure 3(a).

We also compare our results with the uniform refinement strategy. It is emphasized that the regularization parameter has to be decreased accordingly for better reconstruction with finer resolution as we refine the mesh uniformly. In this way can we make the comparison fair for adaptive and uniform refinement strategies. From Figure 4, we see that five adaptive refinements, staring from the initial mesh (448 dofs), result in significant error reduction and reach the convergence plateau afterward by taking into account the essential error in the measurement. On the contrary, the uniform strategy has to use 6112 dofs after two successive uniform refinements to achieve a similar error level as in the $L^2 - L^2$ or $L^2 - H^1$ adaptive schemes with five adaptive refinements with about 1000 dofs. This illustrates clearly enormous advantage of the adaptive reconstruction scheme over the uniform one.

Example 2. (Sharp spike heat flux) The computational domain is a model region of the cross section of a steel furnace, with its outer boundary being an ellipse with x-semi-radius 2 and y-semi-radius 1.5 and its inner boundary being a unit circle. The outer boundary is accessible while the inner boundary is inaccessible. The true distribution of the heat flux has a sharp spike at the point $(0, 1)$ and is given by the 2-D function

$$q(x, y) = \exp(-10(x^2 + (y - 1)^2))$$

restricted on the inner boundary. The true solution u is shown in Figure 5(a). After 10 adaptive refinements from the initial mesh in Figure 5(b), the reconstructed heat flux is approximated very well for both the $L^2 - L^2$ and $L^2 - H^1$ cases as shown in Figure 6(a) and (c), respectively. It is easily seen that the reconstructed heat fluxes capture well the location and height of the sharp spike except some small ripples nearby caused by the amplification of noise. Besides, element refinement is mainly done around the spike from Figure 6(b) and (d).

Example 3. (Dipole-like heat flux) The domain setting is exactly the same as in Example 2, but the heat flux to be constructed here is chosen to be dipole-shaped, which is even more challenging.

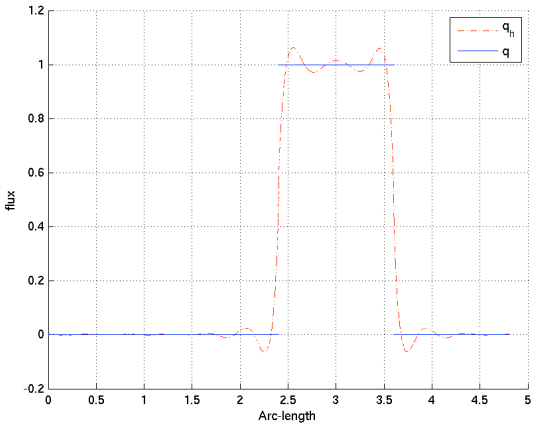

(a) Numerical (red) and true (blue) flux

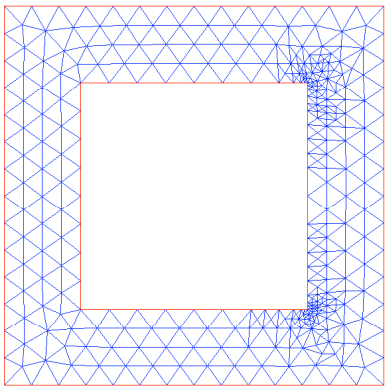

(b) 4 adaptive refinements with 742 dofs

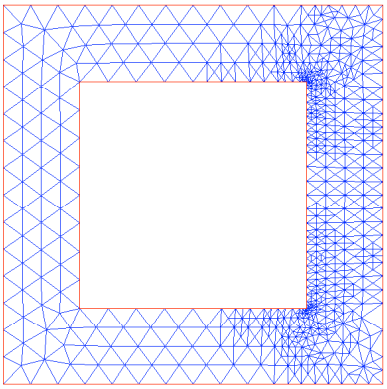

(c) 7 adaptive refinements with 1514 dofs

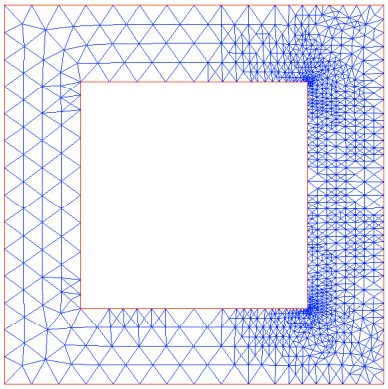

(d) 10 adaptive refinements with 2554 dofs

Figure 2: Numerical reconstruction using the $L^2 - H^1$ error estimator for Example 1.

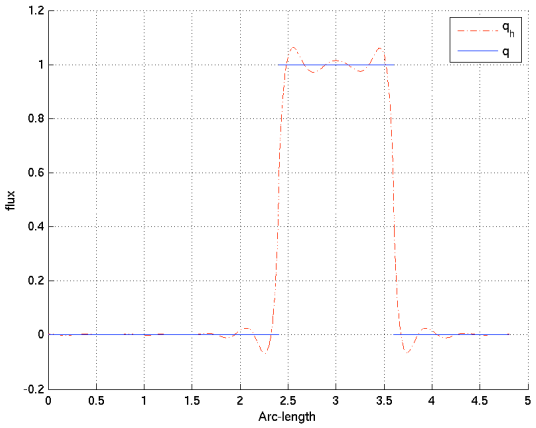

(a) Numerical (red) and true (blue) flux

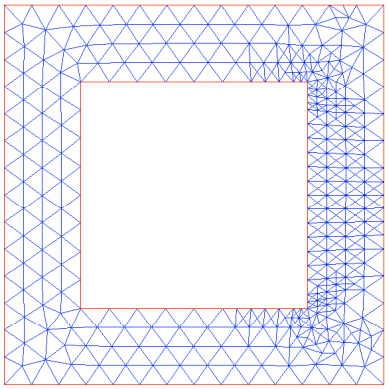

(b) 4 adaptive refinements with 810 dofs

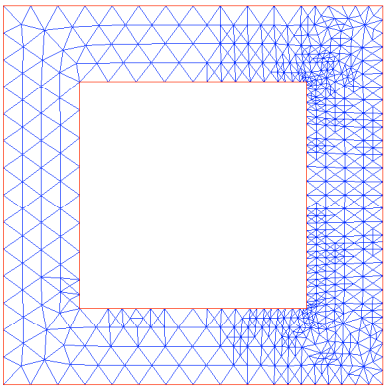

(c) 7 adaptive refinements with 1466 dofs

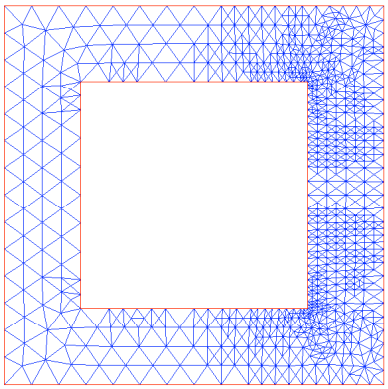

(d) 10 adaptive refinements with 2180 dofs

Figure 3: Numerical reconstruction using the $L^2 - L^2$ error estimator for Example 1.

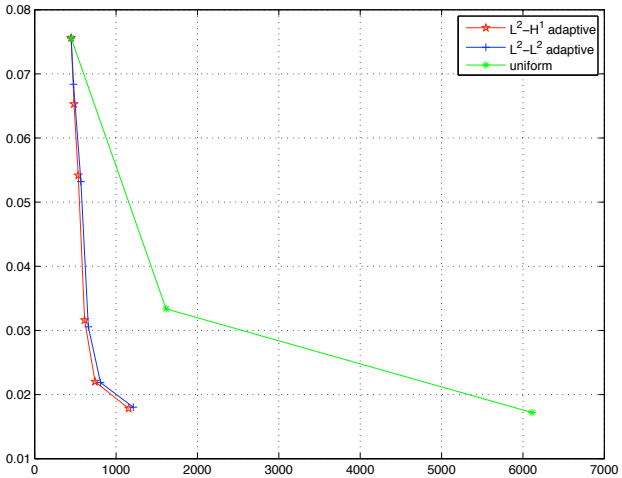

Figure 4: Efficiency comparison for Example 1, adaptive versus uniform strategies.

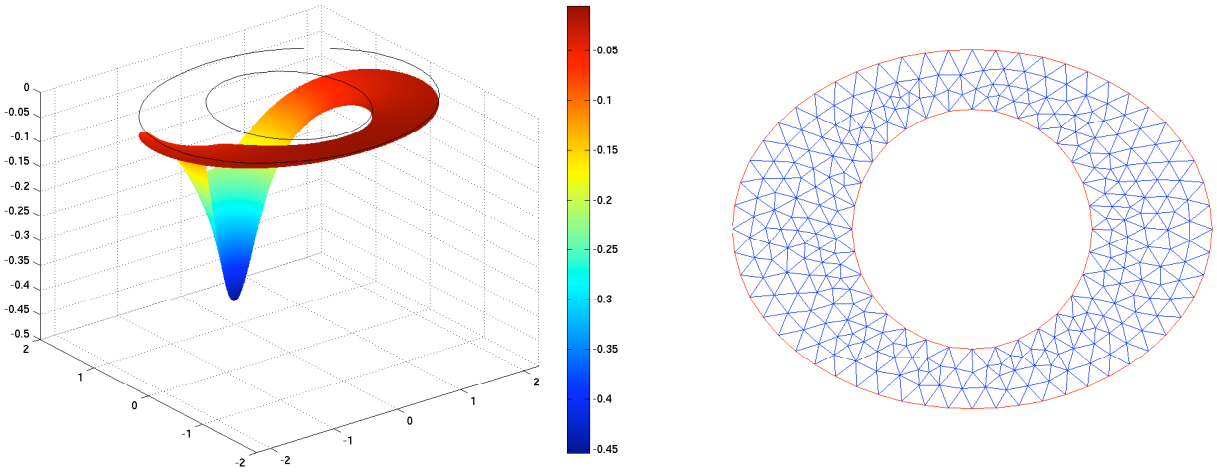

(a) (b)

Figure 5: True solution u (a) and the initial mesh (b) with 634 dofs in Example 2.

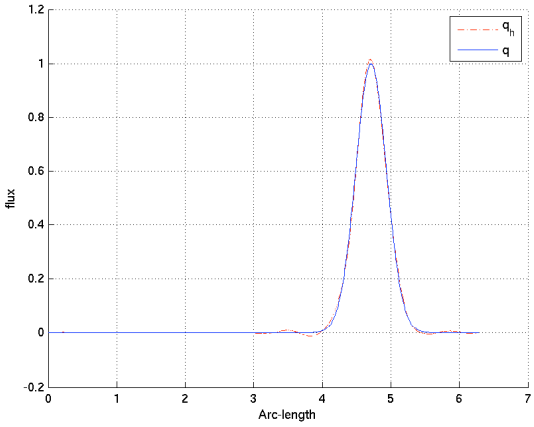

(a) $\|q - q_h\|^2_{0,\Gamma_i} = 3.0849E-4$, $\beta = 1.2E-5$

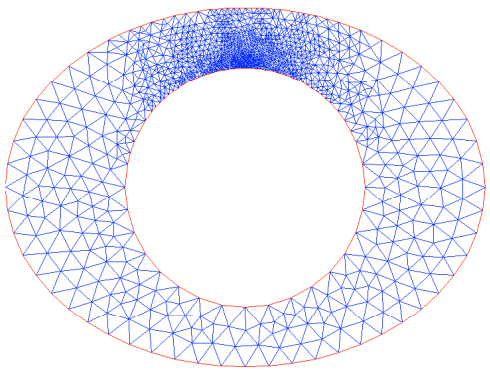

(b) Final mesh with 6059 dofs

$L^2 - H^1$ case

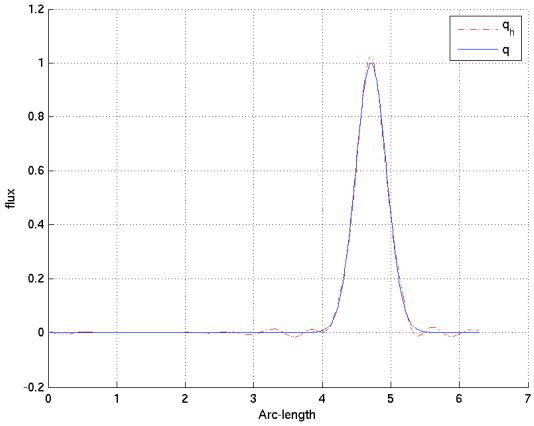

(c) $\|q - q_h\|^2_{0,\Gamma_i} = 6.2355E-4$, $\beta = 0.8E-5$

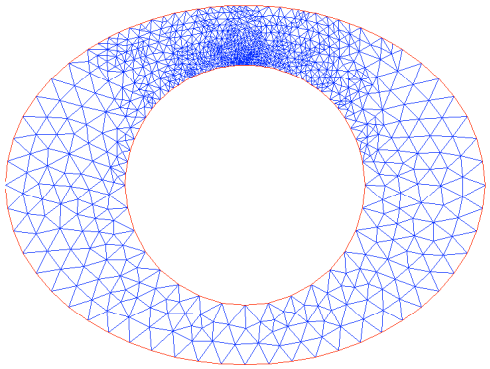

(d) Final mesh with 4407 dofs

$L^2 - L^2$ case

Figure 6: Numerical identified heat fluxes and final meshes in Example 2.

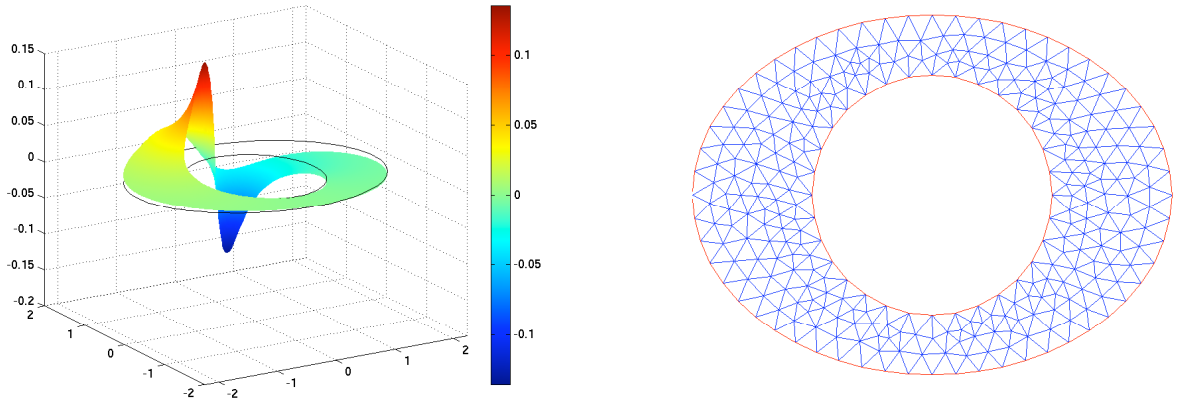

(a) (b)

Figure 7: True solution u (a) and the initial mesh (b) with 634 dofs in Example 3.

The true heat flux has a sharp sign change at the point $(0, 1)$ and given by the 2-D function

$$q(x, y) = \begin{cases} \exp(-10(x^2 + (y-1)^2)) & \text{if } x > 0; \\ -\exp(-10(x^2 + (y-1)^2)) & \text{if } x < 0, \end{cases}$$

restricted on the inner boundary. The true solution u is shown in Figure 7(a). After 15 adaptive refinements from the initial mesh Figure 7(b), the reconstructed heat flux is approximated reasonably well for both the L^2-L^2 and L^2-H^1 cases as shown in Figure 8(a) and (c), respectively. Local feature of the unknown flux is resolved by adaptive refining element around the singular point $(0, 1)$ as shown in Figures 8(b) and (d). It is easily seen that the reconstructed heat fluxes capture well the location and height and even the sharp sign change of the dipole heat flux except small shift of the tips of the dipole flux, which is partly due to the continuous linear elements used to approximate such discontinuous sharp sign-change function q. It is worthnoting that the local feature of the heat flux in this example is highly nontrivial, which requires far more local refinements for better recovering the sharp sign change. Comparison are also made between the uniform and adaptive strategies as shown in Figure 9. To achieve the same flux approximation error (about 0.07 here) before reaching the slow convergence plateau, there are only around 2800 dofs used in the $L^2 - H^1$ scheme and around 2600 dofs used in the $L^2 - L^2$ one, respectively, after six adaptive refinements for the adaptive schemes. Nevertheless, one has to uniformly refine the mesh for three consecutive times, which amounts to approximately 35000 dofs on the final mesh, to obtain similar approximation error. This demonstrates that the more challenging the heat flux, the more efforts can be spared with resort to the adaptive solvers.

5 Conclusions and future work

In this work we have proposed an adaptive finite element method for the inverse problem of distributed heat flux reconstruction in a stationary heat system by deriving the a posteriori error estimators. We have shown the explicit dependence of the upper bound constant of the a posteriori error estimates on the regularization parameter for the first time, which is essential to inverse problems and cannot be dropped. Nevertheless, the a posteriori error estimator is shown to be applicable and efficient irrespective of the adverse amplification effect of the regularization parameter, which deserves further investigation. Moreover, the time-dependent case will be addressed in a forthcoming paper, with adaptive strategy employed both in temporal and spatial dimensions.

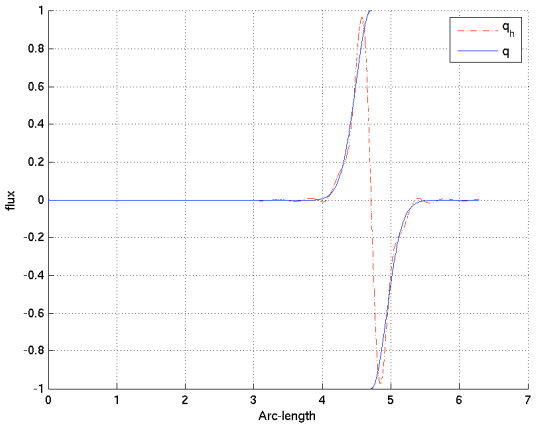

(a) $\|q - q_h\|^2_{0,\Gamma_i} = 6.3282E-2$, $\beta = 2.5E-6$
$L^2 - H^1$ case

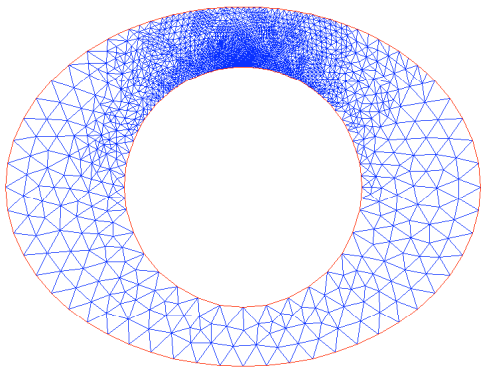

(b) Final mesh with 8135 dofs

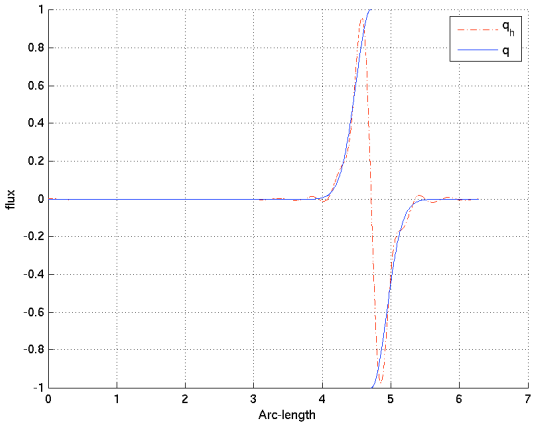

(c) $\|q - q_h\|^2_{0,\Gamma_i} = 6.7241E-2$, $\beta = 1.8E-6$
$L^2 - L^2$ case

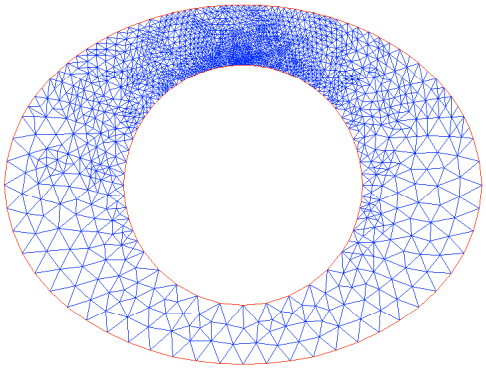

(d) Final mesh with 6870 dofs

Figure 8: Numerical identified heat fluxes and final meshes in Example 3.

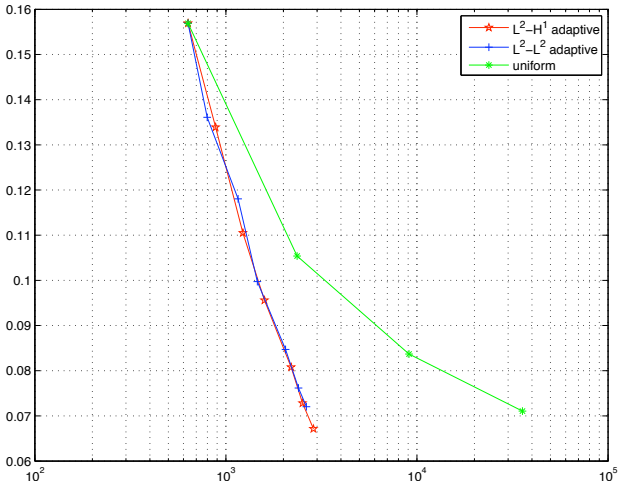

Figure 9: Efficiency comparison for Example 3, adaptive versus uniform strategies.

References

[1] M. Ainsworth and J. T. Oden, A Posteriori Error Estimation in Finite Element Analysis, Wiley, New York, 2000.

[2] O. M. Alifanov, Inverse Heat Transfer Problems. Springer: Berlin, 1994.

[3] I. Babuška and C. Rheinboldt, Error Estimates for Adaptive Finite Element Computations, SIAM J. Numer. Anal., 15 (1978), pp. 736-754.

[4] W. Bangerth and A. Joshi, Adaptive Finite Element Methods for the Solution of Inverse Problems in Optical Tomography, Inverse Problems, 24(3/034011) (2008), pp. 1-22

[5] R. Becker and B. Vexler, A Posteriori Error Estimation for Finite Element Discretization of Parameter Identification Problems, Numer. Math., 96 (2004), pp. 435-459.

[6] L. Beilina and C. Johnson, A Posteriori Error Estimation in Computational Inverse Scattering, Math. Models Methods Appl. Sci., 15 (2005), pp. 23-35.

[7] K. Chrysafinos, M. D. Gunzburger, and L. Hou, Semidiscrete Approximations of Optimal Robin Boundary Control Problems Constrained by Semilinear Parabolic PDE, J. Math. Anal. Appl. 323 (2006), pp. 891-912.

[8] P. G. Ciarlet, The Finite Element Method for Elliptic Problems, North-Holland, Amsterdam, 1978.

[9] E. Divo and J. S. Kapat, Multi-dimensional heat flux reconstruction using narrow-band thermochromic liquid crystal thermography, Inverse Problems in Science and Engineering, 9(5) (2001), pp. 537 - 559.

[10] T. Feng, N. Yan, and W. Liu, Adaptive Finite Element Methods for the Identification of Distributed Parameters in Elliptic Equation, Adv. Comput. Math., 29 (2008), pp. 27-53.

[11] J. Hadamard, Lectures on Cauchy's Problem in Linear Differential Equations. Yale University Press: New Haven, CT, 1923.

[12] A. Kufner, O. John, and S. Fucik, Function Spaces, Nordhoff, Leyden, The Netherlands, 1977.

[13] O. A. Ladyzhenskaya and N. Uraltseva, Linear and Quasilinear Elliptic Equations, Academic Press, New York, 1968.

[14] R. Li, W. Liu, H. Ma, and T. Tang, Adaptive Finite Element Approximation for Distributed Elliptic Optimal Control Problems, SIAM J. Control Optim., 41 (2002), pp. 1321-1349.

[15] J. L. Lions, Optimal Control of Systems Governed by Partial Differential Equations, Springer, Berlin, 1971.

[16] W. Liu, H. Ma, T. Tang, and N. Yan, A Posteriori Error Estimates for Discontinuous Galerkin Time-Stepping Method for Optimal Control Problems Governed by Parabolic Equations, SIAM J. Numer. Anal., 42 (2004), pp. 1032-1061.

[17] W. Liu and N. Yan, A Posteriori Error Estimates for Optimal Control Problems Governed by Parabolic Equations, Numer. Math., 93 (2003), pp. 497-521.

[18] L. R. Scott and S. Zhang, Finite Element Interpolation of Nonsmooth Functions Satisfying Boundary Conditions, Math. Comp., 54 (1990), pp. 483-493.

[19] R. Verfürth, A Posteriori Error Estimators for the Stokes Equations, Numer. Math., 55 (1989), pp. 309-325.

[20] R. Verfürth, A Review of A Posteriori Error Estimation and Adaptive Mesh Refinement Techniques, Teubner, 1996.

[21] J. Xie and J. Zou, Numerical Reconstruction of Heat Fluxes, SIAM J. Numer. Anal., 43 (2005), pp. 1504-1535.

[22] N. Zabaras and S. Kang, On the solution of an ill-posed inverse design solidification problem using minimization techniques in finite and infinite dimensional spaces. Int. J. Numer. Meth. Engng., 36 (1993), pp. 3973-3990.

[23] N. Zabaras and J. Liu, An analysis of two-dimensional linear inverse heat transfer problems using an integral method. Numer. Heat Transfer, 13 (1988), pp. 527-533.

Research Reports

No.	Authors/Title
10-23	*J. Li, J. Xie and J. Zou* An adaptive finite element method for distributed heat flux reconstruction
10-22	*D. Kressner* Bivariate matrix functions
10-21	*C. Jerez-Hanckes and J.-C. Nédélec* Variational forms for the inverses of integral logarithmic operators over an interval
10-20	*R. Andreev* Space-time wavelet FEM for parabolic equations
10-19	*V.H. Hoang and C. Schwab* Regularity and generalized polynomial chaos approximation of parametric and random 2nd order hyperbolic partial differential equations
10-18	*A. Barth, C. Schwab and N. Zollinger* Multi-Level Monte Carlo Finite Element method for elliptic PDE's with stochastic coefficients
10-17	*B. Kågström, L. Karlsson and D. Kressner* Computing codimensions and generic canonical forms for generalized matrix products
10-16	*D. Kressner and C. Tobler* Low-Rank tensor Krylov subspace methods for parametrized linear systems
10-15	*C.J. Gittelson* Representation of Gaussian fields in series with independent coefficients
10-14	*R. Hiptmair, J. Li and J. Zou* Convergence analysis of Finite Element Methods for $H(\mathrm{div};\Omega)$-elliptic interface problems
10-13	*M.H. Gutknecht and J.-P.M. Zemke* Eigenvalue computations based on IDR
10-12	*H. Brandsmeier, K. Schmidt and Ch. Schwab* A multiscale hp-FEM for 2D photonic crystal band
10-11	*V.H. Hoang and C. Schwab* Sparse tensor Galerkin discretizations for parametric and random parabolic PDEs. I: Analytic regularity and gpc-approximation